Numerical Heat Transfer, Part B, 50: 473–489, 2006

ISSN: 1040-7790 print/1521-0626 online
DOI: 10.1080/10407790600682821

Taylor & Francis
Taylor & Francis Group

LEAST-SQUARES SPECTRAL ELEMENT METHOD FOR RADIATIVE HEAT TRANSFER IN SEMITRANSPARENT MEDIA

J. M. Zhao and L. H. Liu
School of Energy Science and Engineering, Harbin Institute of Technology, Harbin, People's Republic of China

Least-squares spectral element method based on the discrete-ordinate equation is developed to solve multidimensional radiative heat transfer problems in semitransparent media. An efficient algorithm for implementation of the method is presented. Chebyshev polynomials are employed as basis functions for the spectral element discretization. The p-convergence characteristics of the least-squares spectral element method are studied. The convergence rate is very fast and approximately follows the exponential law. Four test problems are taken as examples to verify the least-squares spectral element formulation. The predicted temperature distributions and radiative heat flux are determined by the least-squares spectral element method and compared with data in the references. The results show that the least-squares spectral element method developed in this article has good accuracy for solving multidimensional radiative heat transfer problems.

INTRODUCTION

Numerical solution of the radiative transfer equation (RTE) in an absorbing, emitting, and scattering medium requires considerable effort for most practical systems composed of semitransparent media. Recently, many numerical methods have been developed to solve the problem of radiative heat transfer in semitransparent media, such as the Monte Carlo method [1], the zonal method [2], the discrete-ordinates method (DOM) [3–5], the finite-volume method (FVM) [6–10], and the finite-element method (FEM) [11–15]. Among the traditional methods just stated, the FVM and DOM have the ability to treat complex geometry, and are two of the most popular methods to solve the radiative heat transfer in semitransparent media. Recently, many modifications and improvements [16–23] have been made for these two methods, including mitigation of ray effects [16, 17], parallelization [18, 19], and new solution schemes [20–23]. While most of these methods just offer *h* convergence, i.e., the convergence gained by reducing the element size *h* or *h* refinement, as a result, remeshing or refining have to be done in order to gain the wanted accuracy.

Received 29 December 2005; accepted 16 February 2006.
Support of this work by the National Nature Science Foundation of China (50425619, 50336010) is gratefully acknowledged.
Address correspondence to L. H. Liu, School of Energy Science and Engineering, Harbin Institute of Technology, 92 West Dazhi Street, Harbin 150001, People's Republic of China. E-mail: lhliu@hit.edu.cn

NOMENCLATURE

$\Im$	first-order linear differential operator defined in Eq. (4)
h	element size, Lagrange interpolation polynomial defined in Eq. (10)
$\hbar$	two-dimensional spectral nodal basis defined on Ω_{st}^2
$\mathbf{H}$	matrix defined in Eq. (25)
I	radiative intensity
$\tilde{I}$	approximate radiative intensity
I_b	blackbody radiative intensity
$\mathbf{J}$	Jacobian matrix
$\mathbf{K}$	matrix defined in Eq. (24)
L	slab thickness, side length of rectangular medium
M	number of discrete directions
$\mathbf{n}$	inward normal vector
N	number of solution nodes in Ω_{st}^1
N_{el}	total number of elements
N_{esol}	number of solution nodes per element
N_{sol}	total number of solution nodes per element
p	polynomial order
P	Legendre polynomial
q	radiative heat flux, W/m^2
$\mathbf{s}$	unit direction vector
S	source term of radiation transfer equation
T	temperature, K
T_g	medium temperature, K
U^h	global approximation space of spectral element method
V	solution domain
w	weight for S_N approximation, weight defined in Eq. (11)
W	weight function
$\mathbf{x}$	Cartesian coordinate vector defined in solution domain
x, y, z	Cartesian coordinates defined in solution domain
β	extinction coefficient
δ	variable defined in Eq. (11)
ε_w	wall emissivity
$\boldsymbol{\zeta}$	Cartesian coordinate vector defined in standard element
ζ, γ, ς	Cartesian coordinates defined in standard element
Θ	dimensionless temperature
κ	absorption coefficient, m^{-1}
μ^m, ξ^m, η^m	direction cosine of direction m
σ	scattering coefficient, m^{-1}
$\bar{\sigma}$	Stefan-Boltzmann constant, $\text{W/m}^2\,\text{K}^4$
τ_L	optical thickness $[=(\kappa+\sigma)L]$
ϕ	global basis (shape function)
ϕ^e	elemental basis function defined on element e
Φ	scattering phase function
φ	coordinate transform function
Ω_e	general element e
Ω_{st}	standard element
$\nabla_{\mathbf{x}}$	gradient operator with respect to $\mathbf{x}$ $(=\mathbf{i}\frac{\partial}{\partial x}+\mathbf{j}\frac{\partial}{\partial y}+\mathbf{k}\frac{\partial}{\partial z})$
$\nabla_{\boldsymbol{\zeta}}$	gradient operator with respect to $\boldsymbol{\zeta}$ $(=\mathbf{i}\frac{\partial}{\partial \zeta}+\mathbf{j}\frac{\partial}{\partial \gamma}+\mathbf{k}\frac{\partial}{\partial \varsigma})$

Subscripts

e	element index
i	elemental nodal index
i'	transformed elemental nodal index defined in Eq. (14)
n, j	solution node index
w	value at wall boundary

Superscripts

e	function defined on element e
m, m'	direction index
1, 2	dimension

Spectral element approximation, originally proposed by Patera [24] for the solution of fluid problems, combines the advantages of spectral approximation, i.e., the freedom to choose the order p of spectral approximation, offering p convergence, and finite-element approximation, i.e., the flexibility to deal with complex domains and offering h convergence. The p convergence of the spectral element approximation makes it more flexible, and the solution accuracy can be easily increased by just increasing the order or p refinement of spectral approximation without refining or remeshing the geometric mesh. Another very important property of the p convergence is its higher convergence rate, i.e., exponential law for approximating continuous functions. As a result, spectral element approximation is more effective than spectral approximation and finite-element approximation.

Spectral or *hp* finite-element method has been successfully applied to computational fluid dynamics and heat transfer [24–29], and hence it is a natural idea to extend this method to solve radiative transfer problems. Recently, Pontaza and Reddy [30] proposed a least-square *hp* finite-element formulation for solving the one-dimensional integral-differential RTE directly. In their work, two kinds of discretization schemes, namely, space-angle coupled and decoupled schemes are studied, and the results show that the space-angle decoupled scheme is inferior to the space-angle coupled scheme for one-dimensional problems. For multidimensional radiative transfer problems, the space-angle coupled scheme increases the dimension of the solution domain by adding an angular dimension to the spatial dimension and results in very large algebraic equations; it is therefore inefficient. There are also some differences between the solution of 1-D and 2-D or 3-D problems. So it is necessary to develop a space-angle decoupled spectral/*hp* finite-element method and verify its performance for multidimensional radiative transfer problems.

In the present work, we develop a least-squares spectral element method (LSSEM) for solving multidimensional RTEs based on the discrete-ordinates equation of the RTE. An efficient algorithm for implementation of the method is presented. The *p*-convergence characteristics of the least-squares spectral element method are studied. Four test cases of radiative heat transfer in semitransparent media are studied to verify the performance of the method.

MATHEMATICAL FORMULATION

Discrete-Ordinates Equation of the Radiative Transfer Equation

Consider radiative transfer in an enclosure filled with an absorbing, emitting, and scattering gray medium. The discrete-ordinates equation of radiative transfer can be written as

$$\mu^m \frac{\partial I^m}{\partial x} + \eta^m \frac{\partial I^m}{\partial y} + \xi^m \frac{\partial I^m}{\partial z} = \kappa I_b - (\kappa + \sigma) I^m + \frac{\sigma}{4\pi} \sum_{m'=1}^{M} I^{m'} \Phi^{m',m} w^{m'} \tag{1}$$

For the opaque and diffuse boundary, the boundary conditions are given as

$$I_w^m = \varepsilon_w I_{bw} + \frac{1 - \varepsilon_w}{\pi} \sum_{\mathbf{n}_w \cdot \mathbf{s}^{m'} < 0} I_w^{m'} \left| \mathbf{n}_w \cdot \mathbf{s}^{m'} \right| w^{m'} \qquad \mathbf{s}^m \cdot \mathbf{n}_w > 0 \tag{2}$$

For simplicity, the in-scattering term is treated implicitly as part of the source term, thus the original system of partial differential-integral equations transform to a system of partial differential equations of the form

$$\Im^m [I^m] = S^m \tag{3}$$

where

$$\Im^m = \mu^m \frac{\partial}{\partial x} + \eta^m \frac{\partial}{\partial y} + \xi^m \frac{\partial}{\partial z} + (\kappa + \sigma) \tag{4}$$

$$S^m(\mathbf{r}) = \kappa I_b(\mathbf{r}) + \frac{\sigma}{4\pi} \sum_{m'=1}^{M} I^{m'}(\mathbf{r}) \Phi^{m',m} w^{m'} \tag{5}$$

Here, $\Im^m$ is the first-order linear differential operator and S^m is the source term.

The partial differential equation (1) with boundary condition given by Eq. (2) is solved for each discrete direction. Taking direction cosines μ^m, η^m, and ξ^m as velocities in the x, y, and z directions, respectively, operator $\Im^m$ can be considered as a convection operator. Therefore, Eq. (1) is a special case of the general convection-diffusion equation [31]. It is well known that convection-diffusion equations are some of the most difficult problems to solve numerically, especially for convection-dominated problem. The presence of a convection term may cause nonphysical oscillation of solutions. This type of instability can occur in many numerical methods, including the finite-difference method and the finite-element method, if no special stability treatment is taken. In this article, a least-squares spectral element method is developed to solve the discrete-ordinates equation of radiative heat transfer.

Spectral Element Approximation

Spectral element approximation combines the advantages of spectral approximation, i.e., the freedom to choose the order p of approximation, offering p convergence, and finite-element approximation, i.e., the flexibility to deal with complex domains and the freedom to choose element size h, offering h convergence. As in the finite-element method, the solution domain Ω is decomposed into N_{el} nonoverlapping elements Ω_e, that is,

$$\Omega = \bigcup_{e=1}^{N_{\text{el}}} \Omega_e \qquad \bigcap_{e=1}^{N_{\text{el}}} \Omega_e = \emptyset \tag{6}$$

The spectral element method approximates a function by spectral expansion of the function over each element Ω_e. As shown in Figure 1, the spectral bases are originally defined on standard element Ω_{st} and transformed to each general element Ω_e to build basis functions ϕ_i^e over Ω_e. With Lagrange nodal basis expansion, the spectral element approximation can be formulated in a form as in finite-element approximation. Considering the elemental nodal basis as a shape function, the radiative intensity can be approximated over element Ω_e by

$$\tilde{I}^{m,e}(\mathbf{x}) = \sum_{i=1}^{N_{\text{esol}}} I_i^{m,e} \phi_i^e(\mathbf{x}) \tag{7}$$

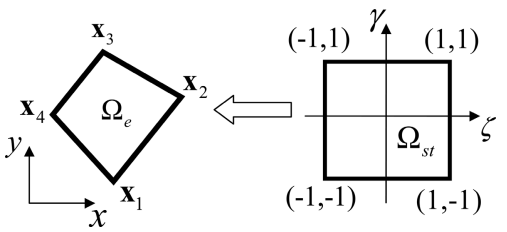

Figure 1. Schematic graph for element coordinate transform.

where $I_i^{m,e}$ denotes the radiative intensity at the ith node of element Ω_e, $\phi_i^e(\mathbf{r})$ are Lagrange nodal basis functions defined on element Ω_e (elemental basis), and N_{esol} denotes the number of solution nodes per element.

Using a global assembly procedure as in the finite-element method, nodal basis functions on each element around node j can be assembled as the global basis (shape function) of node j, denoted by ϕ_j. The global approximation space U^h is taken to be $U^h = \text{span}\{\phi_j, j = 1, \ldots, N_{\text{sol}}\}$. Here, N_{sol} denotes the total number of solution nodes. The global approximation intensity $\tilde{I}^m$ can be written as

$$\tilde{I}^m(\mathbf{x}) = \sum_{j=1}^{N_{\text{sol}}} I_j^m \phi_j(\mathbf{x}) \tag{8}$$

where I_j^m denotes the radiative intensity at solution node j.

In this article, Chebyshev polynomials are used to build the elemental nodal basis function. The $N-1$ order nodal basis functions defined on standard element $\Omega_{\text{st}}^1 = [-1, 1]$ are Lagrange interpolation polynomials through N Chebyshev-Gauss-Lobatto points:

$$\zeta_j = -\cos\left(\frac{j-1}{N-1}\pi\right) \qquad j = 1, \ldots, N \tag{9}$$

By using a barycentric interpolation formula, the Lagrange interpolation polynomials can be written as [32]

$$h_i(\zeta) = \frac{w_i/(\zeta - \zeta_i)}{\sum_{j=1}^N w_j/(\zeta - \zeta_j)} \tag{10}$$

where

$$w_j = (-1)^{j-1}\delta_j \qquad \delta_j = \begin{cases} \frac{1}{2} & j = 1 \text{ or } j = N \\ 1 & \text{otherwise} \end{cases} \tag{11}$$

The barycentric interpolation formula is considered to be accurate and more computationally stable. This is demonstrated in [32–34].

Figure 2 shows the one-dimensional nodal basis for the order of 4. The location of the nodes coincides with the aforementioned Gauss-Chebyshev-Lobatto points. The Kronecker delta property of the nodal basis function is demonstrated in the figure, which ensures that the expansion coefficients in Eqs. (7) and (8) coincide with nodal values and is important to imposing boundary conditions.

Based on the one-dimensional spectral nodal basis function $h_i(\zeta)$, a two-dimensional spectral nodal basis function defined on standard element $\Omega_{\text{st}}^2 = [-1, 1] \times [-1, 1]$ can be built with a tensor product by

$$\hbar_{i,j}(\zeta, \gamma) = h_i(\zeta)h_j(\gamma) \qquad i, j = 1, \ldots, N \tag{12}$$

For the sake of description and implementation, mapping the subscript index of $\hbar_{i,j}$

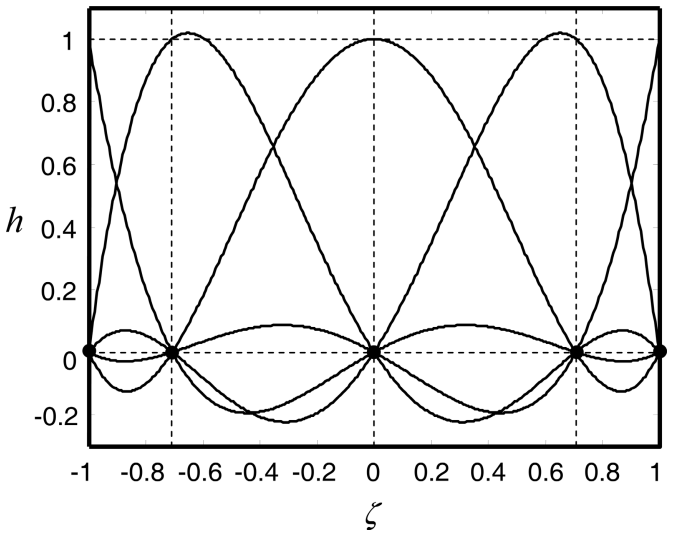

Figure 2. Fourth-order Chebyshev Lagrange interpolation polynomial.

to get a compact form index is needed, i.e., $i' = m(i,j)$, and Eq. (12) can be written as

$$\hbar_{i'}(\zeta,\gamma) = h_i(\zeta)h_j(\gamma) \qquad i' = 1,\ldots,N\times N \tag{13}$$

A simple index mapping pairing used in this article is

$$i' = m(i,j) = (j-1)N + i \tag{14a}$$

$$i = (i'-1)\bmod N + 1 \tag{14b}$$

$$j = \frac{(i'-i)}{N} + 1 \tag{14c}$$

In order to get the elemental nodal basis for general element Ω_e, element transformation is needed. The nodal basis on standard element Ω_{st} and on general element Ω_e is related by

$$\phi^e_{i'}[\mathbf{x}(\boldsymbol{\zeta})] = \hbar^e_{i'}(\boldsymbol{\zeta}) \qquad \mathbf{x}\in\Omega_e, \boldsymbol{\zeta}\in\Omega_{\text{st}} \tag{15}$$

and with derivative relation

$$\nabla_{\mathbf{x}}\,\phi^e_{i'}[\mathbf{x}(\boldsymbol{\zeta})] = \mathbf{J}^{-1}\,\nabla_{\boldsymbol{\zeta}}\,\hbar^e_{i'}(\boldsymbol{\zeta}) \tag{16}$$

where $\mathbf{x} = \mathbf{x}(\boldsymbol{\zeta})$ defines the coordinate transform from Ω_{st} to Ω_e, $\nabla_{\mathbf{x}}$ is the gradient operator with respect to $\mathbf{x}$, $\nabla_{\boldsymbol{\zeta}}$ is the gradient operator with respect to $\boldsymbol{\zeta}$, and $\mathbf{J}$ is the Jacobian matrix.

In this article, the one-dimensional transformation is simply defined by

$$x(\zeta) = \frac{1}{2}[(b-a)\zeta + (a+b)] \tag{17}$$

where $\zeta \in [-1, 1]$ and $x \in [a, b]$. The Jacobian of this transform is just a constant $(b-a)/2$. In two-dimensional cases, the solution domain is decomposed into quadrilateral elements. For each $\boldsymbol{\zeta} \in \Omega_{\text{st}}$, the transformation from standard quadrilateral element Ω_{st} defined by points $\{(-1,-1),(1,-1),(1,1),(-1,1)\}$ to general quadrilateral element Ω_e defined by points $\{\mathbf{x}_1(x_1,y_1), \mathbf{x}_2(x_2,y_2), \mathbf{x}_3(x_3,y_3), \mathbf{x}_4(x_4,y_4)\}$ in anticlockwise order as shown in Figure 1 can be written as

$$x = \sum_{i=1}^{4} x_i \varphi_i(\zeta, \gamma) \tag{18a}$$

$$y = \sum_{i=1}^{4} y_i \varphi_i(\zeta, \gamma) \tag{18b}$$

where

$$\varphi_1(\zeta,\gamma) = \frac{1}{4}(1-\zeta)(1-\gamma) \qquad \varphi_2(\zeta,\gamma) = \frac{1}{4}(1+\zeta)(1-\gamma) \tag{19a}$$

$$\varphi_3(\zeta,\gamma) = \frac{1}{4}(1+\zeta)(1+\gamma) \qquad \varphi_4(\zeta,\gamma) = \frac{1}{4}(1-\zeta)(1+\gamma) \tag{19b}$$

and the Jacobian matrix of this transformation is

$$\mathbf{J} = \frac{\partial(x,y)}{\partial(\zeta,\gamma)} = \begin{bmatrix} \dfrac{\partial x}{\partial \zeta} & \dfrac{\partial y}{\partial \zeta} \\ \dfrac{\partial x}{\partial \gamma} & \dfrac{\partial y}{\partial \gamma} \end{bmatrix} = \begin{bmatrix} a_1 + c_1\gamma & a_2 + c_2\gamma \\ b_1 + c_1\zeta & b_2 + c_2\zeta \end{bmatrix} \tag{20}$$

where

$$a_1 = \frac{1}{4}(-x_1 + x_2 + x_3 - x_4) \qquad a_2 = \frac{1}{4}(-y_1 + y_2 + y_3 - y_4) \tag{21a}$$

$$b_1 = \frac{1}{4}(-x_1 - x_2 + x_3 + x_4) \qquad b_2 = \frac{1}{4}(-y_1 - y_2 + y_3 + y_4) \tag{21b}$$

$$c_1 = \frac{1}{4}(x_1 - x_2 + x_3 - x_4) \qquad c_2 = \frac{1}{4}(y_1 - y_2 + y_3 - y_4) \tag{21c}$$

Discretization of Radiative Transfer Equation

Substituting Eq. (8) into Eq. (3), weighting by $W_j(\mathbf{r})$, and then integrating over the spatial solution domain yields

$$\sum_{n=1}^{N_{\text{sol}}} I_n^m \int_V \Im^m[\phi_n(\mathbf{r})]\, W_j(\mathbf{r})\, dV = \int_V S^m(\mathbf{r})\, W_j(\mathbf{r})\, dV \qquad j = 1, \ldots, N_{\text{sol}} \tag{22}$$

Taking $\Im^m[\phi_j(\mathbf{r})]$ and $\phi_j(\mathbf{r})$ as weight function, we can obtain the least-squares scheme and standard Galerkin scheme of the spectral element method, respectively. Here, only the least-squares scheme of the spectral element method discretization for Eq. (3) is described. Taking $\Im^m[\phi_j(\mathbf{r})]$ as weight function, the following discretized system of linear equations is obtained:

$$\mathbf{K}^m\mathbf{I}^m = \mathbf{H}^m \tag{23}$$

where

$$\begin{aligned} K_{jn}^m = \int_V & \left[\mu^m \frac{\partial\phi_n(\mathbf{r})}{\partial x} + \eta^m \frac{\partial\phi_n(\mathbf{r})}{\partial y} + \xi^m \frac{\partial\phi_n(\mathbf{r})}{\partial z} + (\kappa+\sigma)\phi_n(\mathbf{r})\right] \\ & \times \left[\mu^m \frac{\partial\phi_j(\mathbf{r})}{\partial x} + \eta^m \frac{\partial\phi_j(\mathbf{r})}{\partial y} + \xi^m \frac{\partial\phi_j(\mathbf{r})}{\partial z} + (\kappa+\sigma)\phi_j(\mathbf{r})\right] dV \end{aligned} \tag{24}$$

$$H_j^m = \int_V S^m(\mathbf{r}) \left[\mu^m \frac{\partial\phi_j(\mathbf{r})}{\partial x} + \eta^m \frac{\partial\phi_j(\mathbf{r})}{\partial y} + \xi^m \frac{\partial\phi_j(\mathbf{r})}{\partial z} + (\kappa+\sigma)\phi_j(\mathbf{r})\right] dV \tag{25}$$

By using basis function interpolation, the source term can be expressed as

$$S^m(\mathbf{r}) = \sum_{n=1}^{N} S_n^m \phi_n(\mathbf{r}) \tag{26}$$

If $\beta = (\kappa+\sigma)$ is constant, $\mathbf{K}^m$ and $\mathbf{H}^m$ can be written as

$$\begin{aligned} \mathbf{K}^m = & (\mu^m)^2\mathbf{A}^{xx} + \mu^m\eta^m\mathbf{A}^{xy} + \mu^m\xi^m\mathbf{A}^{xz} + \mu^m\beta\mathbf{B}^{xo} \\ & + \eta^m\mu^m\mathbf{A}^{yx} + (\eta^m)^2\mathbf{A}^{yy} + \eta^m\xi^m\mathbf{A}^{yz} + \eta^m\beta\mathbf{B}^{yo} \\ & + \xi^m\mu^m\mathbf{A}^{zx} + \xi^m\eta^m\mathbf{A}^{zy} + (\xi^m)^2\mathbf{A}^{zz} + \xi^m\beta\mathbf{B}^{zo} \\ & + \beta\mu^m\mathbf{B}^{ox} + \beta\eta^m\mathbf{B}^{oy} + \beta\xi^m\mathbf{B}^{oz} + (\beta)^2\mathbf{B}^{oo} \end{aligned} \tag{27}$$

$$\mathbf{H}^m = (\mu^m\mathbf{B}^{xo} + \eta^m\mathbf{B}^{yo} + \xi^m\mathbf{B}^{zo} + \beta\mathbf{B}^{oo})\mathbf{S}^m \tag{28}$$

Here

$$\begin{aligned} A_{jn}^{xx} &= \int_V \frac{\partial\phi_n(\mathbf{r})}{\partial x}\frac{\partial\phi_j(\mathbf{r})}{\partial x} dV \qquad A_{jn}^{xy} = \int_V \frac{\partial\phi_n(\mathbf{r})}{\partial y}\frac{\partial\phi_j(\mathbf{r})}{\partial x} dV \\ A_{jn}^{xz} &= \int_V \frac{\partial\phi_n(\mathbf{r})}{\partial z}\frac{\partial\phi_j(\mathbf{r})}{\partial x} dV \end{aligned} \tag{29a}$$

$$\begin{aligned} A_{jn}^{yx} &= \int_V \frac{\partial\phi_n(\mathbf{r})}{\partial x}\frac{\partial\phi_j(\mathbf{r})}{\partial y} dV \qquad A_{jn}^{yy} = \int_V \frac{\partial\phi_n(\mathbf{r})}{\partial y}\frac{\partial\phi_j(\mathbf{r})}{\partial y} dV \\ A_{jn}^{yz} &= \int_V \frac{\partial\phi_n(\mathbf{r})}{\partial z}\frac{\partial\phi_j(\mathbf{r})}{\partial y} dV \end{aligned} \tag{29b}$$

$$A_{jn}^{zx} = \int_V \frac{\partial \phi_n(\mathbf{r})}{\partial x}\frac{\partial \phi_j(\mathbf{r})}{\partial z}dV \qquad A_{jn}^{zy} = \int_V \frac{\partial \phi_n(\mathbf{r})}{\partial y}\frac{\partial \phi_j(\mathbf{r})}{\partial z}dV$$
$$A_{jn}^{zz} = \int_V \frac{\partial \phi_n(\mathbf{r})}{\partial z}\frac{\partial \phi_j(\mathbf{r})}{\partial z}dV \tag{29c}$$

$$B_{jn}^{ox} = \int_V \frac{\partial \phi_n(\mathbf{r})}{\partial x}\phi_j(\mathbf{r})\,dV \qquad B_{jn}^{oy} = \int_V \frac{\partial \phi_n(\mathbf{r})}{\partial y}\phi_j(\mathbf{r})\,dV$$
$$B_{jn}^{oz} = \int_V \frac{\partial \phi_n(\mathbf{r})}{\partial z}\phi_j(\mathbf{r})\,dV \tag{30a}$$

$$B_{jn}^{xo} = \int_V \phi_n(\mathbf{r})\frac{\partial \phi_j(\mathbf{r})}{\partial x}dV \qquad B_{jn}^{yo} = \int_V \phi_n(\mathbf{r})\frac{\partial \phi_j(\mathbf{r})}{\partial y}dV$$
$$B_{jn}^{zo} = \int_V \phi_n(\mathbf{r})\frac{\partial \phi_j(\mathbf{r})}{\partial z}dV \tag{30b}$$

$$B_{jn}^{oo} = \int_V \phi_n(\mathbf{r})\phi_j(\mathbf{r})\,dV \tag{30c}$$

The calculation of stiff matrix $\mathbf{K}^m$ can be simplified by noticing the relations

$$\mathbf{A}^{xy} = (\mathbf{A}^{yx})^T \qquad \mathbf{A}^{xz} = (\mathbf{A}^{zx})^T \qquad \mathbf{A}^{yz} = (\mathbf{A}^{zy})^T \tag{31a}$$

$$\mathbf{B}^{ox} = (\mathbf{B}^{xo})^T \qquad \mathbf{B}^{oy} = (\mathbf{B}^{yo})^T \qquad \mathbf{B}^{oz} = (\mathbf{B}^{zo})^T \tag{31b}$$

so only half of these matrices need to be calculated.

It can be seen that the series of matrices **A** and **B** is independent of angular direction. They depend only on the various shape function integration over the solution domain. This means that they need to be assembled only once for each direction. This property can be used to design an efficient algorithm for solving the RTE.

Numerical Implementation

Boundary conditions must be imposed before solving Eq. (23). Here, the collocation technique is used to impose the boundary condition given by Eq. (2). For the Dirichlet boundary condition, the boundary operator can be considered as an identity operator, and it is an identity matrix in discretized form. To impose the boundary condition, we need only to replace the row of stiff matrix $\mathbf{K}^m$ with an index of the boundary node by the corresponding row of the identity matrix, and at the same time, replace the corresponding row of the vector $\mathbf{H}^m$ by the radiation intensity of the boundary node. Thus, for each node j on the inflow boundary of direction m described by Eq. (2), this algorithm can be written as

$$K_{jn}^m = \begin{cases} 1 & j = n \\ 0 & j \neq n \end{cases} \tag{32a}$$

$$H_j^m = I_j^m \tag{32b}$$

Because the source term of the discrete-ordinates equation in direction m contains the radiative intensities of the other directions, global iterations similar to those used in the DOM are necessary to update the source term. The implementation of the least-squares spectral element method can be carried out according to the following routine.

Step 1. Mesh the solution domain with quadrilateral elements.
Step 2. Choose the order of Chebyshev polynomial to build the elemental basis function and generate the solution nodes for each element with Gauss-Chebyshev-Lobatto points.
Step 3. Build the basis function for each element Ω_e from standard element Ω_{st}, integrate to get the element stiff matrix of series of matrices $\mathbf{A}$ and $\mathbf{B}$ defined in Eqs. (29) and (30), then assemble to get the corresponding global stiff matrix of series of matrices $\mathbf{A}$ and $\mathbf{B}$.
Step 4. Begin to loop each angular direction for $m = 1, \ldots, M$, and calculate the corresponding source term matrix $\mathbf{S}^m$, global stiff matrix $\mathbf{K}^m$, and $\mathbf{H}^m$.
Step 5. Impose boundary conditions according to the algorithm described above.
Step 6. Solving the linear equation Eq. (23) to get the radiative intensity on each solution node for angular direction m. End the angular loop.
Step 7. Terminate the iteration process if the stop criterion is satisfied. Otherwise, go back to step 4.

In this article, the maximum relative error 10^{-4} of radiative intensity is taken as stopping criterion for iteration.

RESULTS AND DISCUSSION

To examine the performance of the method presented in this article, four test cases for radiative heat transfer are examined. The test cases are selected because exact or very precise solutions of the radiative transfer equation exist for comparison with the least-squares spectral element method results. The discrete ordinate equation with S_8 approximation is used for all the cases.

Case 1: Nonscattering Gray Medium between Parallel Black Plates

We consider the temperature distribution in a nonscattering gray medium between parallel black plates. The temperatures of the plates are T_1 and T_2, respectively. The least-squares spectral element method was applied to the case with five elements and fourth-order polynomial. The dimensionless temperature distribution $\Theta = (T^4 - T_2^4)/(T_1^4 - T_2^4)$ in the gray medium at radiative equilibrium is presented in Figure 3 for three different optical thicknesses τ_L, namely, 0.1, 1, and 10, and compared with the exact solution obtained by Heaslet and Warming [35]. It can be seen that the least-squares spectral element method results agree with the exact result very well. The maximum error based on the data in [35] is less than 2%.

The polynomial order p on the convergence characteristics of the spectral element solution was studied based on the data in [35]. The relative error was defined as

$$\text{relative error} = \frac{\|\Theta_{\text{LSSEM}} - \Theta_{\text{exact}}\|}{\|\Theta_{\text{exact}}\|} \times 100 \tag{33}$$

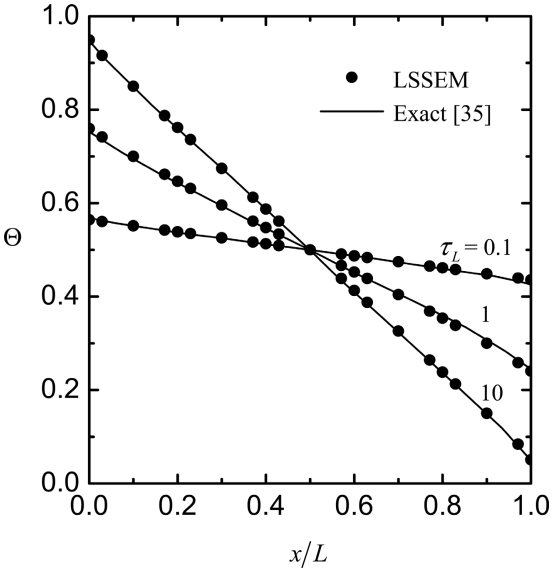

Figure 3. Dimensionless temperature distribution in gray medium at radiative equilibrium.

where $\|\bullet\|$ denotes the l^2 norm, and Θ_{LSSEM} and Θ_{exact} denote the dimensionless temperature distribution obtained by the least-squares spectral element method and the exact data in [35], respectively. The influence of different numerical integration schemes on convergence characteristics was also studied. Here, two spectral elements were used, and both Gauss and Chebyshev-Gauss-Lobatto integration schemes were selected. The relative errors are plotted in Figure 4 for various polynomial orders. It can be seen

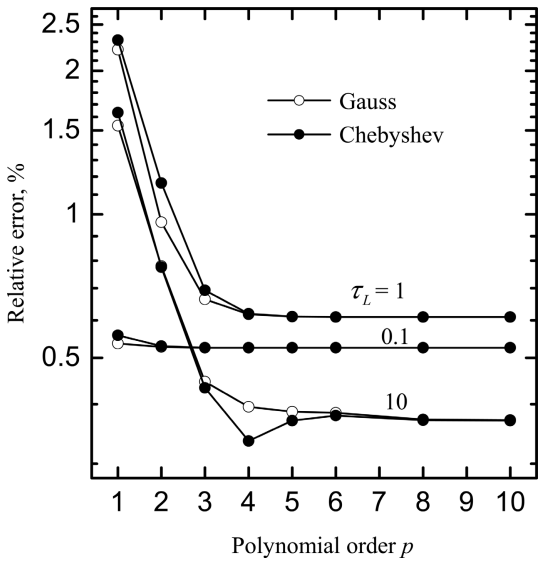

Figure 4. p Convergence on solution of temperature distribution.

that the convergence rate is very fast and approximately follows the exponential law for both integration schemes.

Case 2: Anisotropically Scattering in a Black Enclosure

In this case, we consider radiative heat transfer in a two-dimensional rectangular gray semitransparent medium enclosed by black boundaries. The optical thickness based on the side length L of the rectangular enclosure is $\tau_L = 1.0$. The medium is kept hot, but the temperatures of all boundary walls are maintained at 0 K. The temperature T_g, the absorption coefficient κ, and the scattering coefficient σ of the medium enclosed by the rectangular enclosure are uniform. This case was also studied by Kim and Lee [36] using the DOM. The following phase function [37] with asymmetry factor 0.66972 is used:

$$\Phi = \sum_{j=0}^{8} C_j P_j(\mu) \tag{34}$$

where the P_j are the Legendre polynomials. The C_j are the expansion coefficients defined as $C_0 = 1.0$, $C_1 = 2.00917$, $C_2 = 1.56339$, $C_3 = 0.67407$, $C_4 = 0.22215$, $C_5 = 0.04725$, $C_6 = 0.00671$, $C_7 = 67407$, and $C_8 = 0.00005$.

The least-squares spectral element method was applied to this case for three values of single scattering albedo ω, namely, 0.0, 0.5, and 0.9. Three decomposition schemes, namely, 4, 25, and 49 elements, with fourth-order polynomial are used. The dimensionless net radiative heat fluxes $q_w/\bar{\sigma}T_g^4$ on the lower wall are shown in Figure 5 and compared to the results obtained from DOM [36]. It can be seen that the result is independent of the mesh, and even with four elements the result obtained

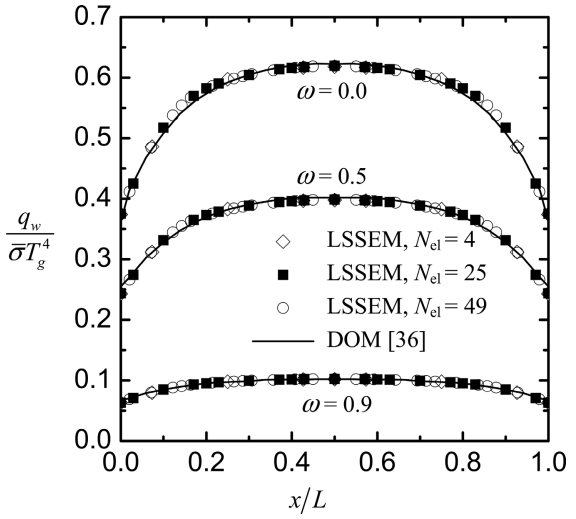

Figure 5. Dimensionless net radiative heat flux on lower wall of rectangular enclosure.

has a good accuracy. The maximum relative error based on the DOM data in [36] is less than 3.5%. The least-squares spectral element method approach presented in this article has good accuracy in solving the radiative heat transfer in anisotropically scattering media.

Case 3: Nonscattering Gray Medium in a Trapezoidal Enclosure

As shown in Figure 6, we consider the radiative heat transfer in a two-dimensional trapezoidal gray semitransparent medium enclosed by black boundaries. The width of the bottom wall is $L = 1$ m. The medium is kept hot, but the temperatures of all boundary walls are maintained at 0 K. The temperature T_g and the absorption coefficient of the medium enclosed by the rectangular enclosure are uniform.

The least-squares spectral element method was applied to this case with fourth-order polynomial and two decomposition schemes, namely, 3 and 27 elements. The solution domain and nodal distribution of the spectral element approximation for three elements is shown in Figure 6. The dimensionless net radiative heat fluxes $q_w/\bar{\sigma}T_g^4$ on the lower wall are shown in Figure 7 for two different values of absorption coefficient, namely, $\kappa = 1.0$ and $\kappa = 0.1\,\mathrm{m}^{-1}$, and compared to the exact solution [38] and the results obtained from the embedded FVM [38]. The maximum relative error based on the exact data in [38] is less than 6% for $N_{\mathrm{el}} = 27$. It can be seen that the least-squares spectral element method approach presented in this article has good accuracy in solving the radiative heat transfer in complex geometries.

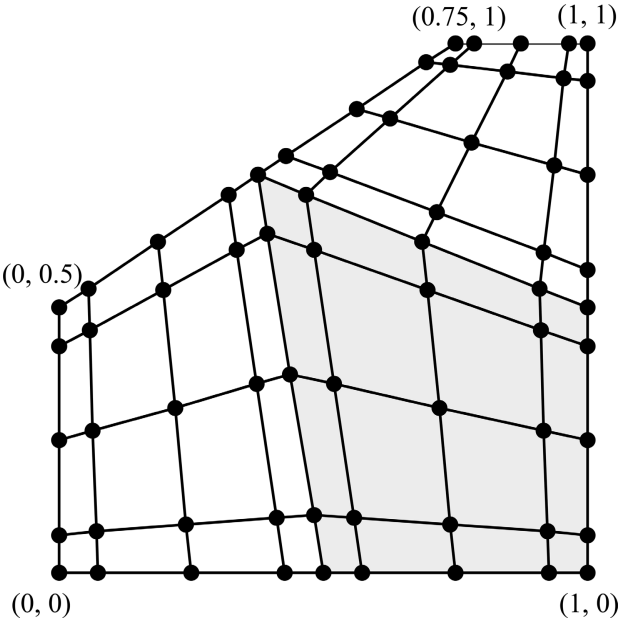

Figure 6. Solution domain and nodal distribution of spectral element approximation for trapezoidal enclosure.

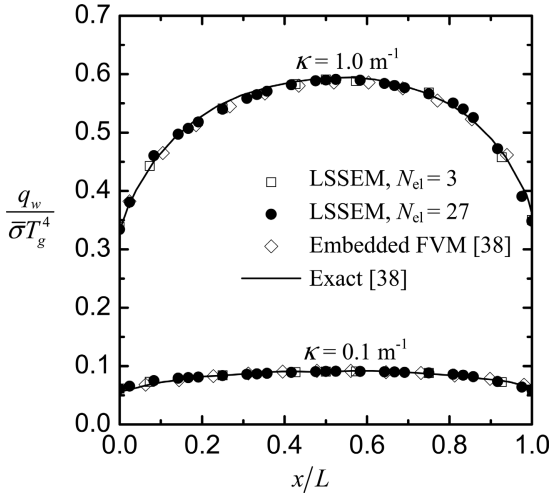

Figure 7. Dimensionless net radiative heat flux on lower wall of trapezoidal enclosure.

Case 4: Isotropically Scattering in a Gray Enclosure

In this case, the least-squares spectral element method is applied to a square enclosure filled by isotropically scattering medium with the single albedo $\omega = 1.0$ and the optical thickness $\tau_L = 1.0$. The lower wall is kept hot, but all other walls and the media enclosed by the rectangular enclosure are kept cold ($T_{w_1} = T_{w_2} = T_{w_3} = T_g = 0\,\mathrm{K}$), which means that the boundary conditions are discontinuous at

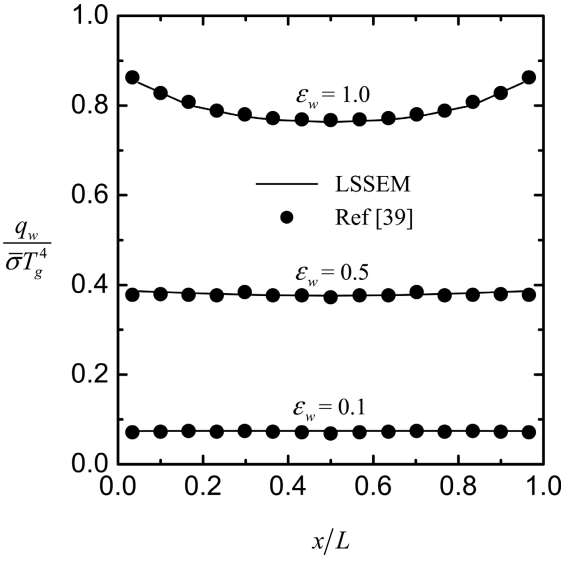

Figure 8. Dimensionless net radiative heat flux on lower wall in gray enclosure filled with purely scattering medium.

the two corners of the lower wall. The least-squares spectral element method was applied to this case with nine elements and fourth-order polynomial. The dimensionless net radiative heat fluxes $q_w/\bar{\sigma}T_{w_1}^4$ on the lower wall are presented in Figure 8 for three values of wall emissivities, namely, 0.1, 0.5, and 1.0, and compared to the results obtained from zone method [39]. It can be seen that the results of the least-squares spectral element method presented in this article agree with those of the zone method very well. Even at blackbody wall condition ($\varepsilon_w = 1.0$), the maximum relative error is less than 1%.

CONCLUSIONS

A least-squares spectral element method based on the discrete-ordinates equation has been developed to solve multidimensional radiative heat transfer problems in semitransparent media. An efficient algorithm for implementation of the method has been presented. Chebyshev polynomials have been employed as basis functions for the spectral element discretization. The *p*-convergence characteristics of the least-squares spectral element method have been studied. The influence of different numerical integration schemes on convergence has also been studied. Gauss and Chebyshev-Gauss-Lobatto integration scheme have been selected. The convergence rate is very fast and approximately follows the exponential law for both integration schemes. Four test problems were taken as examples to verify the least-squares spectral element formulation. The predicted temperature distributions and radiative heat flux were determined by the least-squares spectral element method and compared with data in the references. The results show that the least-squares spectral element method developed in this article has a good accuracy for solving multidimensional radiative heat transfer problems.

REFERENCES

1. J. R. Howell, Application of Monte Carlo to Heat Transfer Problems, *Adv. Heat Transfer*, vol. 5, pp. 1–54, 1968.
2. M. F. Modest, *Radiative Heat Transfer*, McGraw-Hill, New York, 1993.
3. W. A. Fiveland, Discrete-Ordinates Solution of the Radiative Transport Equation for Rectangular Enclosures, *ASME J. Heat Transfer*, vol. 106, pp. 699–706, 1984.
4. S. W. Baek and M. Y. Kim, Modification of the Discrete-Ordinates Method in an Axisymmetric Cylindrical Geometry, *Numer. Heat Transfer B*, vol. 31, pp. 313–326, 1997.
5. K. H. Lee and R. Viskanta, Two-Dimensional Combined Conduction and Radiation Heat Transfer: Comparison of the Discrete Ordinates Method and the Diffusion Approximation Methods, *Numer. Heat Transfer A*, vol. 39, pp. 205–225, 2001.
6. G. D. Raithby and E. H. Chui, A Finite-Volume Method for Predicting a Radiant Heat Transfer in Enclosures with Participating Media, *ASME J. Heat Transfer*, vol. 112, pp. 415–423, 1990.
7. G. D. Raithby, Discussion of the Finite-Volume Method for Radiation, and Its Application Using 3-D Unstructured Meshes, *Numer. Heat Transfer B*, vol. 35, pp. 389–405, 1999.
8. J. C. Chai, H. O. Lee, and S. V. Patankar, Treatment of Irregular Geometries Using a Cartesian Coordinates Finite-Volume Radiation Heat Transfer Procedure, *Numer. Heat Transfer B*, vol. 26, pp. 225–235, 1994.

9. J. C. Chai, One-Dimensional Transient Radiation Heat Transfer Modeling Using a Finite-Volume Method, *Numer. Heat Transfer B*, vol. 44, pp. 187–208, 2003.
10. K. Slimi, L. Zili-Ghedira, N. S. Ben, and A. A. Mohamad, A Transient Study of Coupled Natural Convection and Radiation in a Porous Vertical Channel Using the Finite-Volume Method, *Numer. Heat Transfer A*, vol. 45, pp. 451–478, 2004.
11. W. A. Fiveland and J. P. Jessee, Finite Element Formulation of the Discrete-Ordinates Method for Multidimensional Geometries, *J. Thermophys. Heat Transfer*, vol. 8, pp. 426–433, 1994.
12. L. H. Liu, Finite Element Simulation of Radiative Heat Transfer in Absorbing and Scattering Media, *J. Thermophys. Heat Transfer*, vol. 18, pp. 555–557, 2004.
13. X. Cui and B. Q. Li, A Discontinuous Finite-Element Formulation for Internal Radiation Problems, *Numer. Heat Transfer B*, vol. 46, pp. 223–242, 2004.
14. J. V. Daurelle, R. Occelli, and R. Martin, Finite-Element Modeling of Radiation Heat Transfer Coupled with Conduction in an Adaptive Method, *Numer. Heat Transfer B*, vol. 25, pp. 61–73, 1994.
15. M. Lobo and A. F. Emery, Discrete Maximum Principle in Finite-Element Thermal Radiation Analysis, *Numer. Heat Transfer B*, vol. 24, pp. 209–227, 1993.
16. H. S. Li, G. Flamant, and J. D. Lu, Mitigation of Ray Effects in the Discrete Ordinates Method, *Numer. Heat Transfer B*, vol. 43, pp. 445–466, 2003.
17. J. C. Chai, H. O. Lee, and S. V. Patankar, Ray Effect and False Scattering in the Discrete Ordinates Method, *Numer. Heat Transfer B*, vol. 24, pp. 373–389, 1993.
18. G. Krishnamoorthy, R. Rawat, and P. J. Smith, Parallel Computations of Radiative Heat Transfer Using the Discrete Ordinates Method, *Numer. Heat Transfer B*, vol. 47, pp. 19–38, 2005.
19. J. Con and P. J. Coelho, Parallelization of the Discrete Ordinates Method, *Numer. Heat Transfer B*, vol. 32, pp. 151–173, 1997.
20. N. Sel and I. Ayranci, The Method of Lines Solution of the Discrete Ordinates Method for Radiative Heat Transfer in Enclosures Containing Scattering Media, *Numer. Heat Transfer B*, vol. 43, pp. 179–201, 2003.
21. N. Sel and G. Kirbas, The Method of Lines Solution of the Discrete Ordinates Method for Radiative Heat Transfer in Enclosures, *Numer. Heat Transfer B*, vol. 37, pp. 379–392, 2000.
22. F. Liu, H. A. Becker, and A. Pollard, Spatial Differencing Schemes of the Discrete-Ordinates Method, *Numer. Heat Transfer B*, vol. 30, pp. 23–43, 1996.
23. S. H. Kim and K. Y. Huh, Assessment of the Finite-Volume Method and the Discrete Ordinate Method for Radiative Heat Transfer in a Three-Dimensional Rectangular Enclosure, *Numer. Heat Transfer B*, vol. 35, pp. 85–112, 1999.
24. A. T. Patera, A Spectral Element Method for Fluid Dynamics—Laminar Flow in a Channel Expansion, *J. Comput. Phys.*, vol. 54, pp. 468–488, 1984.
25. G. E. Karniadakis and S. J. Sherwin, *Spectral/hp Element Methods for CFD*, Oxford University Press, Oxford, 1999.
26. R. D. Henderson and G. E. Karniadakis, Unstructured Spectral Element Methods for Simulation of Turbulent Flows, *J. Comput. Phys.*, vol. 122, pp. 191–217, 1995.
27. M. O. Deville, P. F. Fischer, and E. H. Mund, *High-Order Methods for Incompressible Fluid Flow*, Cambridge University Press, Cambridge, 2002.
28. S. Mao, C. A. Luongo, and D. A. Kopriva, Discontinuous Galerkin Spectral Element Simulation of a Thermal-Hydraulic Problem in Superconducting Magnets, *Numer. Heat Transfer A*, vol. 49, pp. 109–127, 2006.
29. C. H. Amon and B. B. Mikic, Spectral Element Simulations of Unsteady Forced Convective Heat Transfer, Application to Compact Heat Exchanger Geometries, *Numer. Heat Transfer A*, vol. 19, pp. 1–19, 1991.

30. J. P. Pontaza and J. N. Reddy, Least-Squares Finite Element Formulations for One-Dimensional Radiative Transfer, *J. Quant. Spectrosc. Radiat. Transfer*, vol. 95, pp. 387–406, 2005.
31. J. C. Chai and S. V. Patankar, Finite-Volume Method for Radiation Heat Transfer, *Adv. Numer. Heat Transfer*, vol. 2, pp. 109–141, 2000.
32. J. P. Berrut and L. N. Trefethen, Barycentric Lagrange Interpolation, *SIAM Rev.*, vol. 46, pp. 501–517, 2004.
33. R. Baltensperger and M. R. Trummer, Spectral Differencing with a Twist, *SIAM J. Sci. Comput.*, vol. 24, pp. 1465–1487, 2003.
34. N. J. Higham, The Numerical Stability of Barycentric Lagrange Interpolation, *IMA J. Numer. Anal.*, vol. 24, pp. 547–556, 2004.
35. M. A. Heaslet and R. F. Warming, Radiative Transport and Wall Temperature Slip in an Absorbing Planar Medium, *Int. J. Heat Mass Transfer*, vol. 8, pp. 979–994, 1965.
36. T. K. Kim and H. Lee, Effect of Anisotropic Scattering on Radiative Heat Transfer in Two-Dimenssional Rectangular Enclosures, *Int. J. Heat Mass Transfer*, vol. 31, pp. 1711–1721, 1988.
37. J. C. Chai, H. S. Lee, and S. V. Patankar, Improved Treatment of Scattering Using the Discrete Ordinates Method, *J. Heat Transfer*, vol. 116, pp. 260–263, 1994.
38. D. Y. Byun, S. W. Baek, and M. Y. Kim, Prediction of Radiative Heat Transfer in a 2D Enclosure with Blocked-off, Multi-block, and Embedded Boundary Treatments, *ASME J. Heat Transfer*, vol. 366, pp. 119–126, 2000.
39. A. C. Ratzel and J. R. Howell, Two-Dimensional Radiation in Absorbing-Emitting Media Using the *P-N* Approximation, *J. Heat Transfer*, vol. 105, pp. 333–340, 1983.